JOURNAL OF GUIDANCE, CONTROL, AND DYNAMICS
Vol. 16, No. 1, January-February 1993

Complex-Frequency Method for Computing the Dynamics of Liquid in a Spinning Container

P. R. Scott*
British Aerospace (Space Systems) Ltd., Stevenage, Herts SG1 4JX, England, United Kingdom
and
D. G. H. Tan†
University of Cambridge, Cambridge CB3 9EW, England, United Kingdom

We present a mathematical model for analyzing the dynamics of liquid in a spinning container. We also indicate how it can be applied to predict the nutation divergence of a spinning spacecraft without knowing the time constant in advance. The response is determined of an inviscid, incompressible fluid to a prescribed, exponentially growing nutational motion of its container. This use of complex frequencies overcomes the mathematical pathologies associated with standard application of the normal mode concept. Two independent numerical algorithms have been developed for the case of completely full, axisymmetric containers. These perform successfully in different but overlapping parameter regimes, within which excellent agreement is found. Results obtained from the algorithms are presented in the form of pressure at the container boundary and overall torque on the container.

I. Introduction

A RECURRENT problem in the design of spacecraft control systems is the destabilizing effect of liquid propellant motion on a spacecraft spinning about its axis of least inertia. Although a rigid body thus spinning is stable, a corresponding body containing fluid is found experimentally[1-3] to be unstable, initially with a small nutation angle exhibiting exponential growth. This occurs even for fluids of low viscosity [in the nondimensional sense defined after Eq. (3) here]. Analyses based on viscous effects (e.g., Orr-Sommerfeld instability[4] or energy dissipation rates) nearly always overestimate the time constant of such growth, by up to two orders of magnitude. We note, in passing, that energy dissipation arguments have proved satisfactory for "dry" spacecraft with flexible appendages.[5] They may also be appropriate for liquid-filled spacecraft in later stages when, for example, turbulent fluid motion has developed.

In this paper, we consider those cases in which there are compelling reasons to believe that the instability arises from inviscid effects, and hence model the fluid as inviscid and incompressible. The theory of inviscid fluid motion does not, of course, include an energy dissipation mechanism, but it does nevertheless admit the possibility of exponential growth of the nutation angle.[6-8] This is because, for a spacecraft spinning about its axis of least inertia, the rotational kinetic energy of the rigid spacecraft can be transferred to the contained fluid by pressure forces, in a manner that conserves both the energy and angular momentum of the combined system.

We also invoke linearized, small-disturbance theory. The approximation used, namely that nonlinear effects are negligible, is valid for sufficiently small departures from an initial state of rigid-body rotation. Such a state is often of interest in spacecraft system design. The exponential growth observed in experiments[1] is consistent with, and highly suggestive of, a linear system.

Received March 26, 1991; revision received Jan. 10, 1992; accepted for publication Feb. 7, 1992.

*Specialist Engineer, Communications Satellites Division. Present address: 25 Chester Road.

†Postdoctoral Research Assistant, Department of Applied Mathematics and Theoretical Physics, Silver Street.

However, attempts to predict the growth time constants from the linearized theory of small-disturbance inviscid fluid motion have often run into difficulties. For example, the linearized, zero-viscosity approximation, when combined with the standard assumption of simple harmonic motion with purely real frequencies, typically leads to a mathematically ill-posed problem[9] and hence, not surprisingly, to erratic numerical behavior.[10-12] We suggest here that this is not a fault of the linearized inviscid approximation itself, nor is it the consequence of the lack of an energy dissipation mechanism, but comes, rather, from applying the standard concept of normal modes (or even forced disturbances) with purely real frequencies. To be sure, the pathology arising from an assumption of purely real frequencies is formally absent when a viscous fluid is considered, but, for realistically small values of viscosity, numerical difficulties are still likely to be encountered.[13]

An alternative and, in this problem, natural approach is to adopt a complex frequency to model the time-dependence of the disturbance, corresponding to exponential growth of the nutation angle. In principle, this leads to well-posed equations, although our results show that, with a sufficiently long time constant, computational difficulties still arise. The use of complex frequencies is related to the Laplace transform approach for initial value problems.[14]

The purposes of the paper are 1) to formulate the complex frequency problem and 2) to present some explicit solutions obtained using two entirely independent numerical methods. In Sec. II, we formulate the linearized equations of motion for an inviscid incompressible fluid completely filling an axisymmetric container that undergoes forced nutation at a prescribed complex frequency. The exact analytic solution of these equations for the particular geometry of a right circular cylinder is expressed as a sum of Bessel functions of complex argument. The two independent numerical methods for computing the disturbance pressure are described in Secs. III and IV; these methods have been implemented for the cylindrical geometry and a more complicated geometry relevant to spacecraft applications. Results from the methods are presented in Sec. V. We address the stability problem in Sec. VI, and we assess the significance of our results in Sec. VII.

II. Formulation

Denote the characteristic scales for position, angular velocity, time, fluid velocity, and fluid pressure by L, Ω, Ω^{-1}, $\epsilon\Omega L$, and $\epsilon\rho\Omega^2L^2$, respectively, where ϵ is a dimensionless number

and ρ the density of the fluid. Let the corresponding nondimensional quantities be $\boldsymbol{x}$, ω, t, $\boldsymbol{u}$, and $\mathrm{Re}\{\tilde{p}\}$, where $\tilde{p}$ is complex-valued and $\mathrm{Re}\{\cdot\}$ denotes the real part of a complex quantity. The notation $\mathrm{Im}\{\cdot\}$ is used later to denote the imaginary part. Consider an inviscid, incompressible fluid completely filling an axisymmetric container that rotates and nutates with a prescribed angular velocity

$$\omega(t) = \mathrm{Re}\left\{\boldsymbol{e}_z + \epsilon A_0(\boldsymbol{e}_r + i\boldsymbol{e}_\theta)\exp\left[i(\theta+\omega_f t)\right]\right\} \tag{1}$$

where $(\boldsymbol{e}_r, \boldsymbol{e}_\theta, \boldsymbol{e}_z)$ are the unit vectors of a cylindrical polar coordinate system rotating with the container ($\boldsymbol{e}_z$ being coincident with the symmetry axis of the container), A_0 is an arbitrary (complex-valued) amplitude, and ω_f is the nondimensional complex forcing frequency. Thus, the real part of ω_f corresponds to the nutation frequency and the imaginary part to the divergence rate. Throughout this section, it is assumed that ω_f is prescribed. Section VI discusses how its value should be varied. Note that the form of Eq. (1) means that the forcing frequencies ω_f, ω_f^*, $-\omega_f$, and $-\omega_f^*$ all describe different motions.

Because the fluid is assumed to completely fill its container, surface tension and gravitation (including centrifugal forces) do not affect the fluid dynamics. We recognize that this is not always valid for practical spacecraft situations but maintain that there are many instances in which the simplification is justifiable.

Relative to the rotating coordinate system, the linearized equations of motion for the fluid velocity (obtained by neglecting terms quadratic in ϵ) are therefore (see Ref. 15, Sec. 2.13)

$$\frac{\partial \boldsymbol{u}}{\partial t} + 2\boldsymbol{e}_z \times \boldsymbol{u} = \mathrm{Re}\left\{-\nabla p' - \epsilon^{-1}\frac{\partial \omega}{\partial t}\times \boldsymbol{x}\right\} \tag{2}$$

where p' is a reduced pressure defined by

$$p' = \tilde{p} - (\omega \times \boldsymbol{x})^2/2\epsilon \tag{3}$$

Equation (2) is the Navier-Stokes equation in a rotating frame of reference without the viscous term $E\nabla^2\boldsymbol{u}$, since the Ekman number E (defined as $\nu/\Omega L^2$, ν being the kinematic viscosity of the fluid) is assumed to be zero for an inviscid fluid. For the practical cases of interest here, E is of the order of 10^{-6}.

By invoking the principle of linear superposition, it is sufficient to assume that $p'(r,\theta,z,t)$ and all other dependent variables (fluid velocity, transverse angular rotation rate, etc.) in the linear problem vary with the same exponentially growing sinusoidal functional dependence. Thus

$$p'(r,\theta,z,t) = p'(r,z)\exp\left[i(\theta+\omega_f t)\right] \tag{4}$$

Introduction of a modified pressure

$$p(r,z) = p'(r,z) + A_0\omega_f rz \tag{5}$$

leads to the velocity $\boldsymbol{u} = (u,v,w)$ being given in terms of p by

$$u = \mathrm{Re}\left\{\exp\left[i(\theta+\omega_f t)\right]\left(1-\frac{\omega_f^2}{4}\right)^{-1} \times\left[\frac{A_0 i\omega_f(\omega_f+2)z}{2} - \frac{i(\omega_f \partial p/\partial r + 2p/r)}{4}\right]\right\} \tag{6}$$

$$v = \mathrm{Re}\left\{\exp\left[i(\theta+\omega_f t)\right]\left(1-\frac{\omega_f^2}{4}\right)^{-1} \times\left[\frac{-A_0\omega_f(\omega_f+2)z}{2} + \frac{(2\partial p/\partial r + \omega_f p/r)}{4}\right]\right\} \tag{7}$$

$$w = \mathrm{Re}\left\{\exp\left[i(\theta+\omega_f t)\right]\left(\frac{i}{\omega_f}\right)\frac{\partial p}{\partial z}\right\} \tag{8}$$

The incompressibility equation $\nabla\cdot\boldsymbol{u} = 0$ then yields a single partial differential equation for $p(r,z)$, namely,

$$\left[r^{-1}\partial_r(r\partial_r) - r^{-2} + (1-4/\omega_f^2)\partial_{zz}\right]p(r,z) = 0 \tag{9}$$

The free-slip boundary condition, $\boldsymbol{u}\cdot\boldsymbol{n} = 0$ at the container walls, takes the form

$$(n_r/r)p(r,z) - (1-\omega_f^2/4)(2n_z/\omega_f)\partial p/\partial z + (n_r\omega_f/2)\partial p/\partial r = A_0\omega_f(\omega_f+2)n_r z \tag{10}$$

where $\boldsymbol{n} = (n_r, 0, n_z)$ is the unit outward normal to the boundary (and is independent of θ for axisymmetric bodies).

It is important to note that, although the differential operator appearing on the left-hand side of Eq. (9) has the same form in the normal mode formulation, the fact that ω_f is complex here means that the differential equation (9), together with the boundary condition (10), is a well-posed boundary value problem. A pair of fourth-order, elliptic differential equations can be obtained for the real and imaginary parts of p, but the boundary conditions remain coupled. (The demonstration of ellipticity has been carried out, but is omitted for brevity.) This should be contrasted with the situation when a real frequency is considered, and this frequency is less than twice the basic spin rate, that is, $\omega_f^2 < 4$, in which case, the differential equation is of the hyperbolic type whereas the boundary condition is of the type normally associated with elliptic partial differential equations. This is the ill-posed mathematical problem referred to in Sec. I.

An analytic solution to Eqs. (9) and (10) is readily derived when the domain is a cylinder $0 \le r \le 1$, $-h \le z \le h$. In this case, the boundary conditions at $z = \pm h$ reduce to $\partial p/\partial z = 0$, and separation of the variables leads to the solution

$$p(r,z) = \sum_{m=0}^{\infty} a_m J_1(\alpha_m r)\sin\left[\frac{(m+\tfrac{1}{2})\pi z}{h}\right] \tag{11}$$

where

$$\alpha_m = \frac{(m+\tfrac{1}{2})\pi(4/\omega_f^2 - 1)^{1/2}}{h} \tag{12}$$

$$a_m = \frac{(-1)^m 4hA_0(\omega_f+2)}{\left[(m+\tfrac{1}{2})\pi\right]^2\left[\alpha_m J_1'(\alpha_m) + (2/\omega_f)J_1(\alpha_m)\right]} \tag{13}$$

and J_1 denotes the Bessel function of the first kind (of complex argument).

Although analytic solutions to Eqs. (9) and (10) can be obtained for other simple container shapes, it seems necessary to resort to numerical techniques when considering the more complicated geometries that arise in practical spacecraft design. We are particularly interested in the propellant tank geometry developed for the Eurostar communications satellite by British Aerospace (Space Systems) Ltd. and MATRA,[16] in which the container consists of a right circular cylinder (of half-height H, say) with hemispherical endcaps (of a radius normalized to unity). (See Fig. 1.) In the next two sections, we describe two independent numerical methods that have been implemented to solve Eqs. (9) and (10) for both the right circular cylinder and Eurostar geometries.

It is of direct relevance to the spacecraft control problem to infer the net torque $\boldsymbol{T}$ exerted by the fluid over the surface S of its rigid container. This vector is given by

$$\boldsymbol{T} = \int_S \boldsymbol{x}\times \mathrm{Re}\{\tilde{p}\}\boldsymbol{n}\,\mathrm{d}S \tag{14}$$

The functional form adopted in Eq. (4) means that $\boldsymbol{T}$ can be resolved in Cartesian coordinates as

$$\boldsymbol{T} = \mathrm{Re}\left\{T(\boldsymbol{e}_x + i\boldsymbol{e}_y)\exp(i\omega_f t)\right\} \tag{15}$$

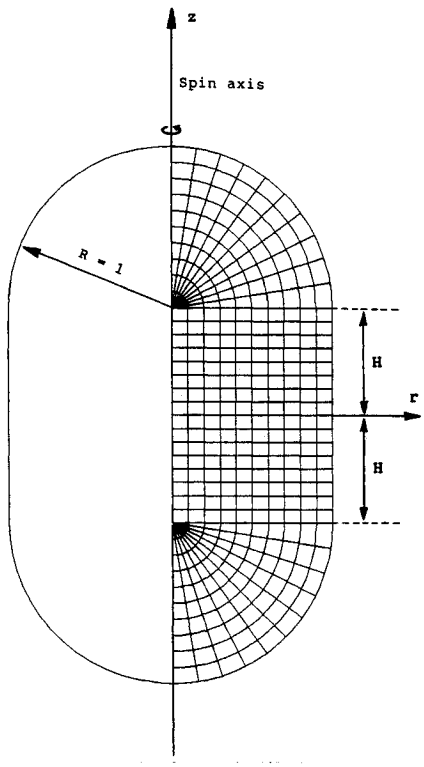

Fig. 1 Section of Eurostar tank showing uniform finite difference mesh.

there being no torque about the z axis in this linearized model. The results given here therefore quote the single complex number T.

III. Polynomial Superposition Method

The solution to Eq. (9) is postulated to have the form

$$p(r,z) = \sum_{n=0}^{N_F-1} b_n p_n(r,z) \tag{16}$$

where

$$p_n(r,z) = \sum_{m=0}^{n} d_{nm} r^{2m+1} z^{2n-2m+1} \tag{17}$$

$$d_{nm} = \frac{(-4/K)^{n-m} n!(n+1)!}{m!(m+1)!(2n-2m+1)!} \tag{18}$$

$$K = 1 - 4/\omega_f^2 \tag{19}$$

and the $\{b_n\}$ are complex amplitude coefficients to be determined. The positive integer N_F denotes the number of such coefficients. These definitions imply that Eq. (9) is satisfied for arbitrary values of the $\{b_n\}$, but to satisfy Eq. (10), it is necessary to make the correct choice of these coefficients. Since Eq. (16) represents a truncated model with only N_F terms, the coefficients are chosen so as to give a "best fit" to the boundary conditions in the following sense.

The coefficients $\{b_n\}$ are selected to minimize

$$\int_C |\boldsymbol{u}\cdot\boldsymbol{n}|^2 \, dC \tag{20}$$

where the integral is taken over the curve C representing the boundary of the container in the (r,z) plane and dC is the arc length. In consequence of Eqs. (6-8), this is equivalent to the minimization of

$$\int_C |L(p)-f|^2 \, dC \tag{21}$$

where L and f are, respectively, the linear operator on the left-hand side and forcing term on the right-hand side of Eq. (10). The determination of the $\{b_n\}$ is thus a standard problem, that is, the unconstrained minimization of a quadratic function. The substitution of Eq. (16) into Eq. (21) leads to the reduction of the minimization problem to the solution of a linear system

$$A\boldsymbol{b} = \boldsymbol{f} \tag{22}$$

where A is a Hermitian matrix whose elements are given by

$$A_{mn} = \int_C [L(p_m)]^* L(p_n) \, dC \tag{23}$$

and f is given by

$$f_m = \int_C [L(p_m)]^* f \, dC \tag{24}$$

In principle, N_F should be made indefinitely large (or increased until further increases have no significant effect on the solution), although in practice this cannot always be achieved since there are constraints on N_F arising from finite numerical precision.

In the numerical results presented in Sec. V, evaluation of the integrals in Eqs. (23) and (24) was performed by Simpson's rule, which has the merit of simplicity as well as being sufficiently accurate for the cases examined. The number of quadrature points on the respective segments of C are M_T and M_U, as indicated in Fig. 2.

The nonsingularity of A has not been checked, except by examining the numerical results. It is easy to see that A is at least positive semidefinite. The linear system (22) was solved by Gaussian elimination with partial pivoting.

IV. Finite Difference Method

In the finite difference formulation, p is solved for approximately at a number of discrete mesh points (r_i, z_j). In the case of a right circular cylinder $0 \le r \le 1$, $-h \le z \le h$, the mesh

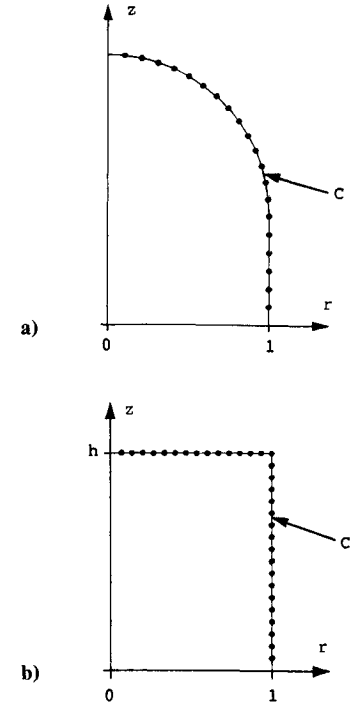

Fig. 2 Quadrature points for polynomial method: a) Eurostar and b) right circular cylinder.

points are uniformly spaced in the cylindrical polar coordinates r and z

$$(r_i,z_j) = (i\Delta r, -h + j\Delta z), \quad i = 1,\ldots,N_R, \quad j = 0,\ldots,N_Z \tag{25}$$

where $\Delta r = 1/N_R$ and $\Delta z = 2h/N_Z$. For $p(r,\theta,z,t)$ as defined in Eq. (4) to be single-valued, we have $p(r,z) = 0$ when $r = 0$. Equations for $p_{i,j}$ are obtained by replacing the differential equation by conventional, second-order, central difference approximations,[17] for example,

$$\frac{\partial^2 p}{\partial r^2}(r_i,z_j) = \frac{(p_{i-1,j} - 2p_{i,j} + p_{i+1,j})}{\Delta r^2} + O(\Delta r^2) \tag{26}$$

At the rigid boundary $r = 1$, an alternative expression is employed, namely,[17]

$$\frac{\partial^2 p}{\partial r^2}(r_{N_R},z_j) = 2(p_{N_R-1,j} - p_{N_R,j})/\Delta r^2 + (2/\Delta r)\partial p/\partial r(r_{N_R},z_j) + O(\Delta r^2) \tag{27}$$

and an expression for $\partial p/\partial r(r_{N_R},z_j)$ is obtained from the boundary condition (10). An analogous procedure is employed at the boundaries $z = \pm h$, and placing the discrete unknowns in a vector, say, $\boldsymbol{p}$, results in a system of linear simultaneous equations

$$A\boldsymbol{p} = \boldsymbol{b} \tag{28}$$

The matrix A is sparse, but its elements are complex-valued and it is not Hermitian, $A^\dagger \neq A$. The solution $\boldsymbol{p}$ is found by applying the conjugate gradient method[18] to the system $A^\dagger A\boldsymbol{p} = A^\dagger \boldsymbol{b}$ and is equivalent to minimizing $(A\boldsymbol{p} - \boldsymbol{b})^\dagger(A\boldsymbol{p} - \boldsymbol{b})$. The conjugate gradient method has the attractive features of exploiting the sparsity of A and also of being guaranteed to converge within N iterations in exact arithmetic, where N is the dimension of the vector $\boldsymbol{p}$. It should be noted, however, that the condition number of $A^\dagger A$ is worse than that of A, which can cause the method to converge less rapidly than might be hoped. This can be expected to be more troublesome for small values of $|\,\mathrm{Im}\{\omega_f\}\,|$, corresponding to slow exponential growth rates.

For the Eurostar geometry, the same discretization scheme is employed in the cylindrical section, but in the hemispheres a mesh with uniform spacing in spherical polar coordinates is used (refer to Fig. 1). This has the advantage of simplifying the discretization of the boundary conditions and merely requires the differential equation to be re-expressed in terms of spherical polar coordinates (which is achieved by a straightforward change of variables). In Sec. V, the integers N_R, N_Z, and N_P refer to the number of points along the radial, axial, and polar lines, respectively.

V. Results

The results presented here are intended to indicate the extent to which computations from our two numerical methods agree with each other and with the analytic solution where available. We know of no experimental measurements of pressure or torque with which to compare our results. All results were computed using 16 (decimal) digit precision and had $A_0 = 1$. The right circular cylinder results pertain to the case $h = 4/3$. For the Eurostar results, the half-height H of the cylindrical section is 2/3 (see Fig. 1).

In addition to tabulating calculations of the torque T defined by Eq. (15), we also present plots of the time-varying component of disturbance pressure $\tilde{p}$ at the container boundary. The real and imaginary parts of $\tilde{p}$ represent the

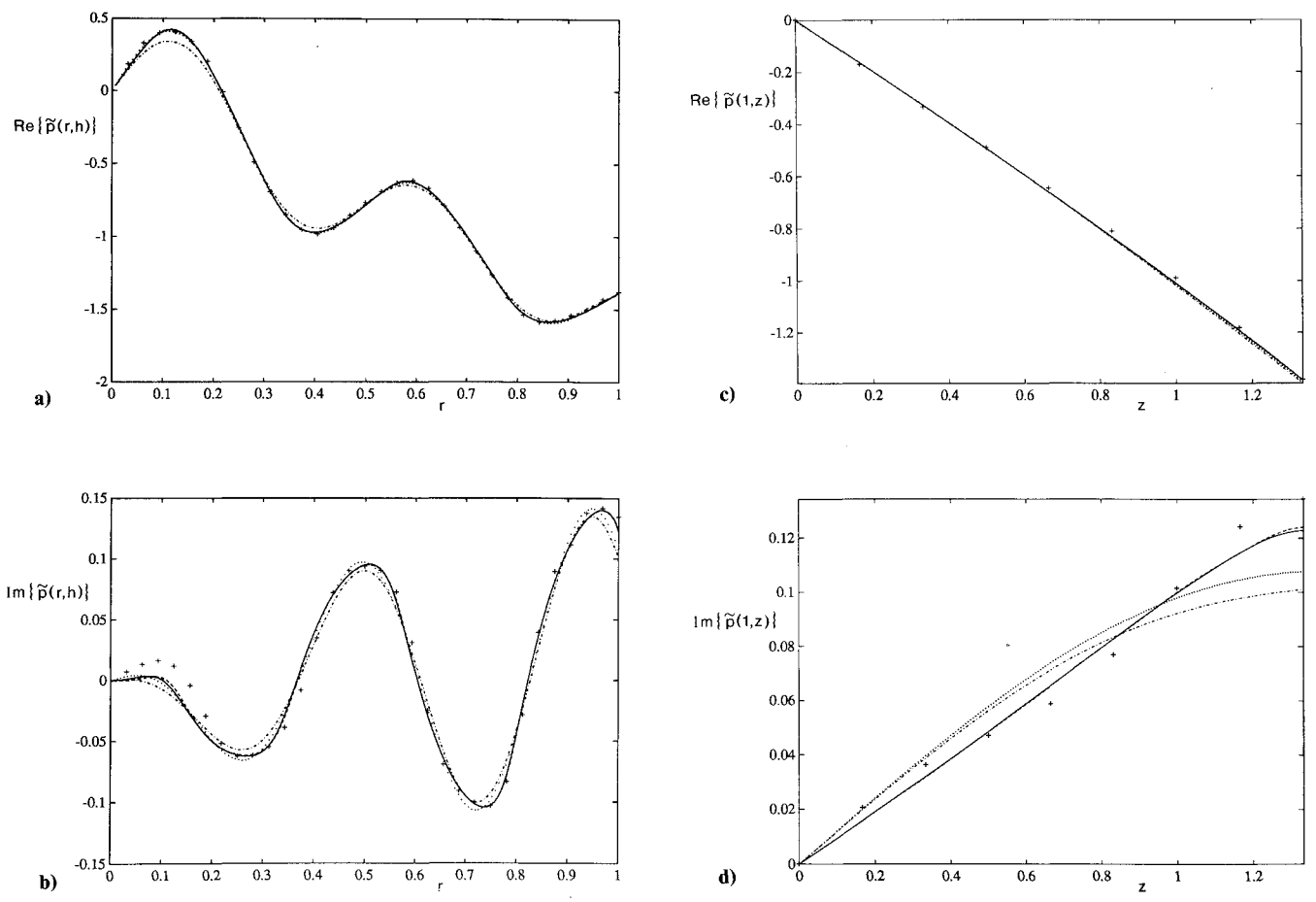

Fig. 3 Boundary pressure for right circular cylinder subject to forcing frequency $\omega_f = 0.167284 - 0.006978i$.

Table 1 Torque values from pressure fields in right circular cylinder ($h = 4/3$)[a]

ω_f	(N_R, N_Z)	(N_F, M_T, M_U)	T
$-1.5-1.0i$	Analytic		$-2.0372+3.6220i$
	(32,32)		$-2.0350+3.6183i$
	(64,64)		$-2.0368+3.6210i$
		(13, 150, 200)	$-2.0374+3.6218i$
$1.5-1.0i$	Analytic		$-1.8123-2.7821i$
	(32,32)		$-1.8154-2.7815i$
	(64,64)		$-1.8140-2.7820i$
		(13, 150, 200)	$-1.8136-2.7823i$
$-0.167284-0.006978i$	Analytic		$-1.3647+2.6028i$
	(64,33)		$-1.3864+2.6508i$
	(128,67)		$-1.3705+2.6141i$
		(9, 150, 200)	$-1.0664+2.6351i$
		(13, 150, 200)	$-1.3635+2.6034i$
$0.167284-0.006978i$	Analytic		$0.4200+2.5049i$
	(32,16)		$0.4333+2.4866i$
	(128,67)		$0.4207+2.5027i$
		(9, 150, 200)	$0.3917+2.5496i$
		(13, 150, 200)	$0.4147+2.5103i$

[a]For definitions of finite difference resolution (N_R, N_Z) and polynomial method parameters (N_F, M_T, M_U), see main text.

pressure field at $t=0$ as a function of r and z when the phase is $\theta=0$ and $-\pi/2$, respectively.

For the right circular cylinder geometry and with a sufficiently large divergence rate, both the polynomial and finite difference methods lead to well-conditioned numerical equations that yield results in excellent agreement with the analytic solution. Two examples of this are for the cases $\omega_f = \pm 1.5 - 1.0i$. Plots of boundary pressure produced by the polynomial method with $N_F = 13$, $M_T = 150$, $M_U = 200$ and by the finite difference method with modest resolution ($N_R = 64$, $N_Z = 64$) both agree with the analytic solution to better than the linewidth of our plotting device and are consequently not shown. The finite difference method was found to be robust to systematic changes in resolution. The torque values T resulting from the numerical computations are given in Table 1.

To make a critical assessment of both numerical methods, we now consider a case that is close to the ill-posed, real frequency problem, namely, $\omega_f = 0.167284 - 0.006978i$. The pressure at the boundary specified by the analytic solution is shown as the solid curves in Fig. 3. Figures 3a and 3b show the real and imaginary parts of $\tilde{p}$ at $z=h$, whereas Figs. 3c and 3d correspond to $r=1$. Different vertical scales have been employed in the graphs so that discrepancies can be more easily identified.

The finite difference method was applied with a coarse mesh, $N_R = 32$, $N_Z = 16$, and the computed values are portrayed as + signs in Fig. 3. Truncation error has led to appreciable inaccuracies in $\mathrm{Im}\{\tilde{p}\}$. To reduce these, it was necessary to increase the resolution to $N_R = 128$, $N_Z = 67$, resulting in the dashed curves in Fig. 3. These curves are almost indistinguishable from the analytic solution.

The dash-dot and dotted curves in Fig. 3 are the results obtained from the polynomial method with $N_F = 9$ and 13, respectively. No improvement was obtained when N_F was increased beyond 13, probably due to the increasing effect of roundoff errors. It can be seen that the polynomial method slightly misplaces the turning points of $\mathrm{Im}\{\tilde{p}(r,h)\}$ (see Fig. 3b). Furthermore, it fails to accurately emulate the curvature of $\mathrm{Im}\{\tilde{p}(1,z)\}$ (see Fig. 3d). Similar behavior is observed for the case $\omega_f = -0.167284 - 0.006978i$.

The values given in Table 1 show that, despite producing noticeably different pressure fields, the different computations all produce similar torques. Thus, although all computations give similar predictions for the overall dynamics of the rigid container, they predict rather different fluid flows. This could have serious implications when assessing the significance of viscous and nonlinear effects.

It should be noted that the right circular cylinder is a special geometry for which normal modes exist. For the case $h = 4/3$, there are modes of relatively low spatial order with eigenfrequencies $\lambda = -0.165713$ and 0.188647. It has been confirmed that the solutions for the complex forcing frequencies $\omega_f = \pm 0.167284 - 0.006978i$ are dominated by these. For complex forcing frequencies close to eigenfrequencies of modes of higher spatial complexity, it is to be expected that the solutions have correspondingly greater complexity.

We now address the Eurostar tank geometry with forcing frequency $\omega_f = -1.5 - 1.0i$. The finite difference and polynomial methods yield pressure fields that are in close agreement with each other. Only the polynomial method result with $N_F = 15$ has been plotted in Fig. 4 because the others are indistinguishable. The solid and dashed curves are the real and imaginary parts of $\tilde{p}$, respectively, plotted as a function of arc length (measured from $r=1$, $z=0$) along the boundary curve C. There is no analytic solution available for comparison. Finite difference solutions at five different resolutions have been computed and found to vary in a manner consistent with errors that are second-order in mesh size. This is in accordance with theory. Torque values are listed in Table 2.

For $\omega_f = +1.5 - 1.0i$, equally good agreement has been obtained. The pressure plots are omitted for reasons of brevity, but the torque values are still listed in Table 2.

VI. Stability Analysis of Spinning Liquid-Filled Spacecraft

So far, the value of ω_f has been assumed to be prescribed. We indicate here how to infer those values of ω_f that determine the stability or otherwise of a spinning liquid-filled spacecraft. Let the rigid spacecraft have inertia tensor $\mathfrak{I}$. The torque required to sustain rigid-body motion with angular velocity $\omega(t)$ is given by what is often referred to as Euler's equation (see Ref. 19, Sec. 5.5)

$$T_r = \mathfrak{I} \cdot \frac{\partial \omega}{\partial t} + \omega \times \mathfrak{I} \cdot \omega \tag{29}$$

Consider first a spacecraft for which e_z is one principal inertia axis and suppose the two transverse inertias are equal. Denote the axial and transverse inertias by $\epsilon^{-1} I_z$ and $\epsilon^{-1} I_x$, respectively. When $\omega(t)$ is given by Eq. (1), the required torque is of the form

$$T_r = \mathrm{Re}\{T_r(\omega_f)(e_x + ie_y)\exp(i\omega_f t)\} \tag{30}$$

where

$$T_r(\omega_f) = A_0 i\left[I_z + I_x(\omega_f - 1)\right] \tag{31}$$

When the dynamics of the rigid spacecraft and its contained fluid are considered together, such motion can only be sustained by application of an external torque T_e, given by

$$T_e = \mathrm{Re}\{T_e(e_x + ie_y)\exp(i\omega_f t)\} \tag{32}$$

where $T_e(\omega_f)$ is defined by

$$T_e(\omega_f) = T_r(\omega_f) - T(\omega_f) \tag{33}$$

Any value of ω_f that satisfies

$$T_e(\omega_f) = 0 \tag{34}$$

defines a motion of the coupled spacecraft-fluid system that is possible in the absence of external torques. Equation (34) can therefore be considered a nonlinear eigenvalue problem. Any solution with $\mathrm{Im}\{\omega_f\} < 0$ corresponds to an unstable mode. Of great interest is the mode with the fastest growth rate.

In determining the stability or otherwise of a spacecraft with prescribed inertias, all solutions of the nonlinear equation (34) must be determined. The use of our numerical methods to compute $T(\omega_f)$, and hence $T_e(\omega_f)$, is sufficiently robust and computationally efficient to permit evaluation at many trial values of ω_f, provided that the trial growth rates are large enough. Thus, iterative schemes can be devised to accurately locate solutions of Eq. (34). One scheme that has been implemented begins by making a broad sweep of the complex ω_f plane to identify the approximate location of each solution. Subsequently, a form of Newton's method is used to locate each solution more accurately (partial derivatives being evaluated numerically).

A particular solution of Eq. (34) can be derived in the last case of Table 1, $\omega_f = 0.167284 - 0.006978i$. With $A_0 = 1$, the analytic solution for p gives $T = 0.4200 + 2.5049i$. Thus, Eq. (34) is satisfied if and only if $I_x = 60.19$ and $I_z = 52.625$. Dimensional inertias can be obtained by multiplying I_x and I_z by ρL^5. Thus, we have a well-defined prediction that a spacecraft with these inertia values, and a single full cylindrical tank mounted concentrically with the center of mass, is capable of initially diverging at the specified rate through the inviscid action of the contained liquid.

This approach can be extended to handle cases of axisymmetric tanks in spacecraft with unequal transverse inertias, but it is then necessary to generalize the circular motion described by Eq. (1) to elliptical nutation. This can be achieved by taking a linear combination of two circular motions (with frequencies ω_f and $-\omega_f^*$) so that the numerical methods described in this paper can still be used.

VII. Conclusions

In this paper we have presented a conceptual framework for analyzing the destabilizing effect of liquid propellant motion on nutating spacecraft that avoids the mathematical difficulties of the normal-mode approach. Our method abandons the notion of free normal-mode motion and substitutes the notion of exponentially growing disturbances forced by the exponentially growing nutational motion of the rigid container. We have devised and implemented two independent numerical methods to compute the disturbance pressure in axisymmetric containers. The methods produce excellent agreement with each other and with the exact analytic solution for a right circular cylinder, provided that the exponential growth rate is sufficiently large. We have indicated how this work can be extended to determine the nutation divergence time constant of a rotating spacecraft carrying liquid fuel. It should be remembered that the present analysis considers completely filled axisymmetric containers and is based on assumptions of linearized, small-disturbance inviscid fluid motion. Although the available data suggest this is reasonable for the practically important initial phases of nutation divergence, the effects of surface tension, gravitation (including centrifugal forces), nonlinearity, and viscosity will become increasingly significant at later times and in the behavior of real spacecraft under active nutation control.

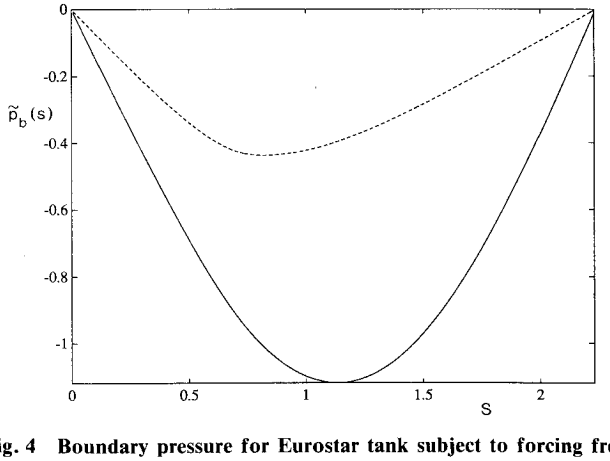

Fig. 4 Boundary pressure for Eurostar tank subject to forcing frequency $\omega_f = -1.5 - 1.0i$.

Table 2 Torque values from pressure fields in Eurostar tank ($H = 2/3$)[a]

ω_f	(N_R, N_Z, N_P)	(N_F, M_T, M_U)	T
$-1.5-1.0i$	(128,128,127)		$-1.6363+4.1655i$
		(10,210,90)	$-1.6357+4.1651i$
		(15,210,90)	$-1.6360+4.1654i$
$1.5-1.0i$	(128,128,127)		$-1.2536-2.4545i$
		(10,210,90)	$-1.2533-2.4542i$
		(15,210,90)	$-1.2535-2.4545i$

For definitions of finite difference resolution (N_R, N_Z, N_P) and polynomial method parameters (N_F, M_T, M_U), see main text.

Acknowledgments

This work was supported by Royal Aeronautical Establishment Contract SLS/32A 1814 and SERC grant GR/G/56317. The idea of using complex frequencies was suggested independently to us by M. E. McIntyre. L. M. Hocking suggested the closely related Laplace transform approach. We thank J. C. Jackson, P. F. Linden, and R. Manasseh for many illuminating discussions.

References

[1]Pocha, J. J., "Final Report on a Drop Test Programme Conducted for the RAE," British Aerospace (Space Systems) Ltd., Tech. Rept. TP8203, Stevenage, Hertfordshire, England, Sept. 1985.

[2]Garg, S. C., Furumoto, N., and Vanyo, J. P., "Spacecraft Nutational Instability Prediction by Energy-Dissipation Measurements," *Journal of Guidance, Control, and Dynamics,* Vol. 9, No. 3, 1986, pp. 357-362.

[3]Harrison, J. V., "Analysis of Spacecraft Nutation Dynamics Using the Drop Test Method," *Space Communication and Broadcasting,* Vol. 5, Sept. 1987, pp. 265-280.

[4]Schlichting, H., *Boundary Layer Theory,* Pergamon, London, 1955, Chap. 16.

[5]Bracewell, R. N., and Garriott, O. K., "Rotation of Artificial Earth Satellites," *Nature,* Vol. 182, Sept. 20, 1958, pp. 760-762.

[6]Greenhill, A. G., "On the General Motion of a Liquid Ellipsoid Under the Gravitation of Its Own Parts," *Proceedings of the Cambridge Philosophical Society,* Vol. 4, Oct. 1980, pp. 4-14.

[7]Rumyantsev, V. V., "Stability of Motion of Solid Bodies with Liquid-Filled Cavities by Lyapunov's Method," *Advances in Applied Mechanics,* Vol. 8, 1964, pp. 183-232.

[8]Stewartson, K., "On the Stability of a Spinning Top Containing Liquid," *Journal of Fluid Mechanics,* Vol. 5, May 1959, pp. 577-592.

[9]Høiland, E., "Discussion of a Hyperbolic Equation Relating to Inertia and Gravitational Fluid Oscillations," *Geofisiska Publikationes,* Vol. 24, June 1962, pp. 211-227.

[10]Scott, P. R., and Matthews, N. F., "Propellant Sloshing Study

Final Report," British Aerospace (Space Systems) Ltd., Tech. Rept. TP8138, ESTEC Contract 5414/83/NL/BI(SC), Stevenage, Hertfordshire, England, July 1984.

[11]McIntyre, J. E., and Tanner, T. M., "Fuel Slosh in a Spinning On-Axis Propellant Tank: An Eigenmode Approach," *Space Communication and Broadcasting,* Vol. 5, Sept. 1987, pp. 229–251.

[12]Henderson, G. A., "A Finite Element Method for Inertial Waves in a Frustum," MSc. Thesis, Faculty of Graduate Studies, Centre for Research in Earth and Space Science, York Univ., North York, Ontario, July 1988.

[13]Heuser, G. E., Ribando, R. J., and Wood, H. G., "A Numerical Simulation of Inertial Waves in a Rotating Fluid," *Computer Methods in Applied Mechanics and Engineering,* Vol. 57, Aug. 1986, pp. 207–222.

[14]Stewartson, K., and Roberts, P. H., "On the Motion of a Liquid in a Spheroidal Cavity of a Precessing Rigid Body," *Journal of Fluid Mechanics,* Vol. 17, Sept. 1963, pp. 1–20.

[15]Greenspan, H. P., *The Theory of Rotating Fluids,* Cambridge Monographs on Mechanics and Applied Mathematics, Cambridge, Univ. Press, Cambridge, England, 1968, p. 69.

[16]Pocha, J. J., "An Experimental Investigation of Spacecraft Sloshing," *Space Communication and Broadcasting,* Vol. 5, Sept. 1987, pp. 323–332.

[17]Smith, G. D., *Numerical Solution of Partial Differential Equations,* Oxford Univ. Press, London, 1965, Chap. 1.

[18]Fletcher, R. W., *Practical Methods of Optimization. Vol. 1: Unconstrained Optimization,* Wiley, Chichester, England, 1980, pp. 63–69.

[19]Goldstein, H., *Classical Mechanics,* 2nd ed., Addison-Wesley, Reading, MA, 1980, p. 204.